Characteristic plasmon energies for 2D In_2Se_3 phase identification at nanoscale

Changsheng Chen[a]+, Minzhi Dai[b]+, Chao Xu[a], Xiangli Che[a], Christian Dwyer[c], Xin Luo[b], and Ye Zhu[a]**

[a]Department of Applied Physics, Research Institute for Smart Energy, The Hong Kong Polytechnic University, Hung Hom, Hong Kong, China

[b]State Key Laboratory of Optoelectronic Materials and Technologies, Guangdong Provincial Key Laboratory of Magnetoelectric Physics and Devices, Centre for Physical Mechanics and Biophysics, School of Physics, Sun Yat-sen University, Guangzhou 510275, China

[c]Electron Imaging and Spectroscopy Tools PO Box 506, Sans Souci, NSW 2219, Australia

KEYWORDS: Chalcogenides, 2D Materials, EELS, Plasmon, Phase identification.

ABSTRACT: Two-dimensional (2D) materials with competing polymorphs offer remarkable potential to switch the associated 2D functionalities for novel device applications. Probing their phase transition and competition mechanisms requires nanoscale characterization techniques that can sensitively detect the nucleation of secondary phases down to single-layer thickness. Here we demonstrate nanoscale phase identification on 2D In_2Se_3 polymorphs, utilizing their distinct plasmon energies that can be distinguished by electron energy-loss spectroscopy (EELS). The characteristic plasmon energies of In_2Se_3 polymorphs have been validated by first-principles calculations, and also been successfully applied to reveal phase transitions using in situ EELS. Correlating with in situ X-ray diffraction, we further derive a subtle difference in the valence electron density of In_2Se_3 polymorphs, consistent with their disparate electronic properties. The nanometer resolution and independence of orientation make plasmon-energy mapping a versatile technique for nanoscale phase identification on 2D materials.

Polymorphism in two-dimensional (2D) materials forms an exciting frontier not only to explore new phases with exotic functionalities at reduced dimensionality, but also to manipulate these 2D functionalities through controlled phase switching for novel device applications. The most prominent examples have been 2D metal chalcogenides,[1,2] in which the medium electronegativity of chalcogen elements (S, Se and Te) leads to competing ionic and covalent bonding, further giving rise to polymorphs with distinct bonding configurations.[1] It manifests as the well-known 2H, 1T and 1T' phases in transition-metal dichalcogenides (TMDs), and more recently as the α and β' phases in 2D In_2Se_3. Despite the fascinating opportunities on fabricating controllable phase-change devices, these competing polymorphs can also intermix in an uncontrollable manner,[3,4] making single-phase synthesis challenging. Resolving the 2D polymorphs is thus of particular importance both for understanding the phase switching mechanism such as the nucleation of the second phase, and for evaluating the purity of the samples. Conventional characterization techniques such as X-ray diffraction (XRD) and Raman spectroscopy do not have sufficient resolution to detect nanoscale intergrowth of polymorphs. Atomic-resolution transmission electron microscopy (TEM) can identify various polymorphs on the unit cell level, but requires them to be on the zone axes that can be difficult to achieve for nanoscale second phases.

In this work, we demonstrate a nanoscale phase identification on 2D In_2Se_3 polymorphs, utilizing their distinct plasmon energies that can be distinguished by electron energy-loss spectroscopy (EELS). As a chalcogenide semiconductor in the III_2-VI_3 family, In_2Se_3 is polymorphic with many phases reported (α', α, β', β, γ, δ, κ).[5-10] The two room-temperature phases, α- and β'-In_2Se_3, and the high-temperature β phase have the 2D layered structure consisting of [Se-In-Se-In-Se] quintuple layers with several possible stacking orders (2H, 3R, 1T).[4,7,11,11] Within each quintuple layer, β'- and β-In_2Se_3 have all the In atoms octahedrally coordinated by Se atoms, whereas α-

In_2Se_3 have only one layer of In atoms octahedrally coordinated and the other In layer with tetrahedral coordination (Figure 1a).[4] More excitingly, α-In_2Se_3 exhibits 2D ferroelectricity that is currently under intensive investigation,[10,14-19] while β'-In_2Se_3 possesses a 2D antiferroelectric superstructure that distinguishes it from the high-temperature paraelectric β phase.[20] The rich polymorphism makes In_2Se_3 a fascinating system for exploring both the fundamental ferroelectric physics at the 2D limit and ultrathin phase-switching device applications.[15,16,18,19,21-23] On the other hand, with similar stability of polymorphs, In_2Se_3 has been reported to possess intermixed phases on the nanometer level,[3,4] which can be difficult to distinguish. Here we show that In_2Se_3 polymorphs exhibit disparate plasmon energies that can be experimentally detected by EELS and also verified by first-principles calculations. It makes plasmon-energy mapping an effective technique for phase identification down to single-layer thickness, relatively independent of sample orientation (in contrast to atomic-resolution TEM). We further demonstrate it on studying In_2Se_3 phase transitions using correlative in situ EELS and XRD, which unveils a subtle difference in the valence electron density of In_2Se_3 polymorphs.

We prepare α-In_2Se_3 and β'-In_2Se_3 flakes in 2H and 3R stacking by mechanical exfoliation on commercially available crystals (see Experimental Section in Supporting Information (SI)). Figure 1 summarizes the characterization techniques that can distinguish the four In_2Se_3 phases, by their distinct atomic structure in cross-section scanning TEM (STEM, Figure 1a) or spectroscopic signals in Raman spectroscopy (Figure 1c) and X-ray diffraction (XRD, Figure 1d). More interestingly, we discover that the four phases exhibit slightly different plasmon energies (E_p) that can be sensitively detected by low-loss EELS. As shown in Figure 1b, despite the similar shape of plasmon peaks comprising two peaks at ~15 and 21 eV, there is a subtle shift of the first plasmon peak between the four phases as indicated by the vertical dash-dotted line. Using least-square curve

fitting, we have extracted E_p quantitatively, which follows the order E_p(α-2H) < E_p(α-3R) < E_p(β'-2H) < E_p(β'-3R) (see Table S1 in SI). Even though the shifts are small compared with the peak width, they can be consistently measured in both [0001] and <11$\bar{2}$0> orientations (Figure 1b).[24] The shifts between 2H and 3R In_2Se_3 (~0.15 eV) are generally smaller than those between α and β' phases (~0.35 eV), both are within the sensitivity of modern EELS spectrometers. The identified E_p and its shifts are relatively independent of sample thickness and surface effect, as demonstrated in Figure S12 and S13.

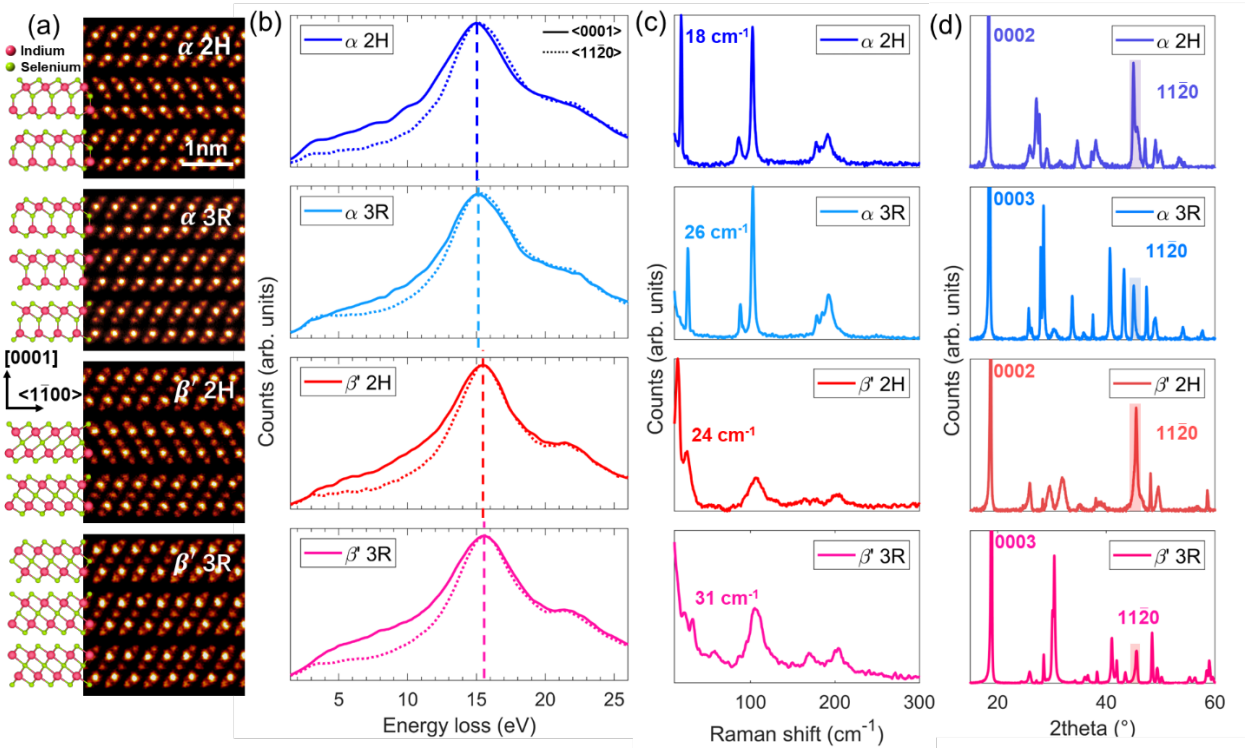

Figure 1. (a) Atomic-resolution Z-contrast STEM images along <11$\bar{2}$0> zone axis with the structural model shown on the left. (b) Low-loss EEL spectra taken along [0001] and <11$\bar{2}$0> zone axes with the plasmon energies indicated by dashed lines. The higher intensity at 3-12 eV in [0001] EEL spectra compared to <11$\bar{2}$0> spectra in (b) is consistent with higher absorption of [0001]-polarized light compared to in-plane-polarized light. (c) Raman spectra and (d) XRD at room temperature for the four In_2Se_3 phases, respectively.

The detected E_p difference have been explicitly verified by first-principles calculations (see Experimental Methods) as presented in Figure 2. Based on the calculated dielectric functions [ϵ_1 and ϵ_2], the derived energy-loss function Im(-1/ϵ) quantitatively matches the experimental low-loss spectra in Figure 1b, with both plasmon peaks reproduced in the proper shape at the correct energies (Figure 2, Figure S7, and Figure S8). The ~0.5 eV energy shift of the first plasmon peak between α- and β-In_2Se_3 is also reproduced, providing theoretical validation that measuring E_p using low-loss EELS can be used to distinguish α- and β'-In_2Se_3. On the other hand, the calculated E_p differences between 2H and 3R stacking of the same In_2Se_3 phase are negligible. It may imply an insufficient understanding on the stacking structure of In_2Se_3, which requires further investigation. We note that compared with XRD and Raman spectroscopy, EELS in STEM can reach sub-nanometer resolution even using the low-loss signal,[25] thus offering a powerful technique for nanoscale phase identification on In_2Se_3.

The capability of nanoscale phase mapping using low-loss EELS is experimentally demonstrated in Figure 3. Owing to the competition between various phases, second-phase intergrowths are often present in In_2Se_3, with an example shown in Figure 3a. Here the intergrowth is β'-In_2Se_3 only three layers thick embedded in α-In_2Se_3 lattice (Figure 3b), which can be clearly mapped out in Figure 3c by its higher E_p compared with the α-In_2Se_3 matrix. The atomically sharp α/β' interfaces become ~1.1 nm wide as revealed by the energy profile in Figure 3c, evidencing the nanometer resolution of E_p mapping that should be limited by the size of probe and the delocalization of the low-loss EELS signal.[25,26] Although not comparable to TEM/STEM imaging, this resolution is still sufficient to detect the thinnest intergrowth, i.e., single-quintuple-layer In_2Se_3 (~1 nm wide). Another example of resolving two-layer β'-In_2Se_3 intergrowth in α-In_2Se_3 is presented in Figure S3. Moreover, with the same trend of E_p in both [0001] and $<11\bar{2}0>$ orientations (Figure 1b), E_p

mapping does not suffer the restriction of sample orientations that is required by TEM/STEM imaging, and thus is more applicable to general samples with random orientation of second-phase intergrowths.

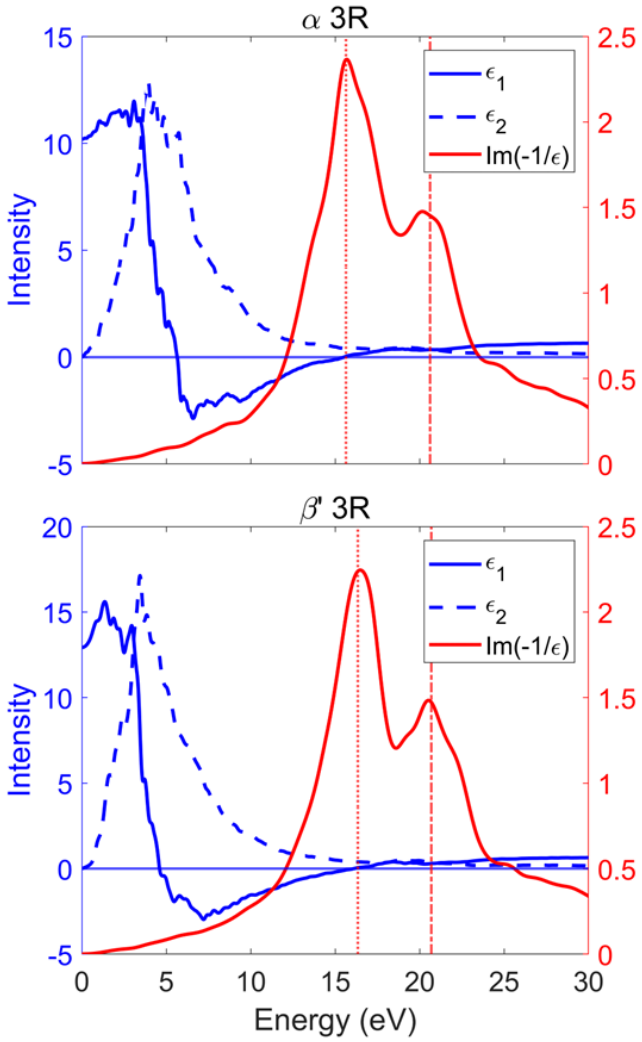

Figure 2. Calculated real (blue solid) and imaginary parts (blue dash) of the dielectric functions, and energy-loss functions (red solid) for α-3R (upper) and β'-3R (bottom) In_2Se_3, respectively, with vertical dotted lines and dash-dotted lines indicating the plasmon peak positions.

The observed E_p difference can also be utilized to study phase transitions between In_2Se_3 polymorphs. Using *in situ* heating/cooling in STEM to induce phase transition, we measure E_p as functions of temperatures as shown in Figure 4a. Two major features can be observed: *i*) the linear decrease of E_p with increasing temperature for all four phases, which maintains their E_p difference at various temperatures; and *ii*) the leap from the lower E_p of α-2H/3R phases to the higher E_p of β-2H/3R In_2Se_3 at ≥250 °C corresponding to α-to-β transition. There is no E_p leap for the transition between β'- and β-In_2Se_3, which can be attributed to their same basic structure except for the additional antiferroelectric ordering in β'-In_2Se_3 (Figure S8).[20] The phase transitions between α-, β'- and β-In_2Se_3 has also been verified by electron diffraction during *in situ* heating (Figure S6). Both above features validate the observed E_p difference in Figure 1b. We note that *in situ* EELS experiment presented in Figure 4a has been repeated three times with good reproducibility (Figure S5).

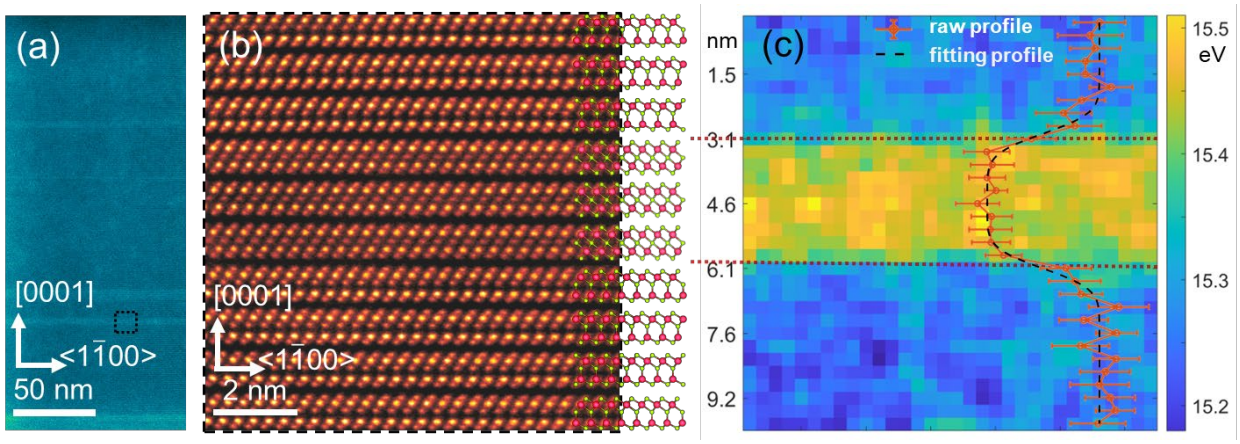

Figure 3. (a) Low-magnification image of an α-3R In_2Se_3 flake with the intergrowth of β'-In_2Se_3 as the bright straight lines. (b) Atomic-resolution Z-contrast STEM image from the squared region in (a), showing three quintuple layers of β'-In_2Se_3 inserted in α-3R In_2Se_3 lattice. (c) Plasmon-energy mapping using low-loss EELS with the horizontally averaged energy profile overlaid, which can detect the 3-nm-wide β'-In_2Se_3 intergrowth.

The linear decrease of E_p with increasing temperature has been reported for other 2D chalcogenides,[27,28] which can be explained by the well-known dependence of E_p on valence electron density n through the formula:

$$E_p(T) = \hbar\sqrt{\frac{n(T)e^2}{\epsilon_0 m_{eff}}} = \hbar\sqrt{\frac{n_0}{V(T)}\frac{e^2}{\epsilon_0 m_{eff}}}, \quad (1)$$

where $\hbar$ is reduced Plank constant, ϵ_0 is the vacuum permittivity, e and m_{eff} are charge and effective mass of an electron, $n(T)$ is the valence electron density $n(T) = n_0/V(T)$, and n_0 is the number of valence electrons within the volume $V(T)$. Raising temperature causes thermal expansion and decreases $n(T)$, as reflected by the monotonic decrease of $E_p(T)$ in Figure 4a, which has been utilized to perform nanoscale measurements of temperature[29] and thermal expansion coefficients.[27] The temperature-dependent volume variation can be quantitatively derived by measuring lattice parameters using *in situ* XRD. As depicted in Figure 4b, the single-quintuple-layer unit-cell volumes $V(T)$ increases linearly with temperature, corresponding to thermal expansion for all four phases. The linear temperature dependence of $V(T)$ suggests that In_2Se_3 thermal expansion is dominated by the linear thermal expansion coefficient,[30-32] which has been fitted and listed in Table S2. Combining Figure 4a and 4b, we can use Equation 1 to calculate n_0 as plotted in Figure 4c (see Note 1 in SI): n_0 of all four In_2Se_3 phases shows no obvious temperature dependence, which indicates that the observed linear decrease of $E_p(T)$ in Figure 4a is completely due to thermal expansion.

More interestingly, Figure 4c unveils an intrinsic difference in the number of valence electrons n_0 of the four phases. From Equation 1, the first plasmon peak at ~15 eV corresponds to $n_0 \approx 23$ valence electrons (per In_2Se_3 formula-unit), which is a subset of totally 44 outer-shell electrons of In_2Se_3. Figure 4c further illustrates that β'/β-In_2Se_3 possesses ~0.5 more valence electron than α-In_2Se_3 when comparing the same stacking structure (2H or 3R). It shows that the measured E_p

difference between various phases in Figure 4a is not only caused by the volume effect, i.e., V(α-2H) > V(α-3R) > V(β'-2H) > V(β'-3R) as shown in Figure 4b, but also reflecting their different n_0 with n_0(α-2H) < n_0(α-3R) < n_0(β'-2H) < n_0(β'-3R) as shown in Figure 4c. We note that n_0 here is derived from Equation 1 based on the simple free-electron model, which may be interpreted as a simplified indicator of the electronic properties. The more valence electrons in β'/β-In_2Se_3 are indeed consistent with their higher conductivity compared with α-In_2Se_3,[12,33,34] which could arise from the more octahedral coordination in β'/β-In_2Se_3 which has been demonstrated to be relatively unstable.[35]

In summary, we demonstrate nanoscale phase identification on 2D In_2Se_3 polymorphs using E_p mapping based on low-loss EELS. The characteristic E_p of In_2Se_3 polymorphs is validated by first-principles calculations and can be applied to reveal phase transitions using *in situ* EELS. Correlating with *in situ* X-ray diffraction, we further derive a subtle difference in the valence electron density of In_2Se_3 polymorphs, consistent with their electronic properties. The nanometer resolution and independence of orientation make E_p mapping a versatile technique for nanoscale phase identification on emerging materials.

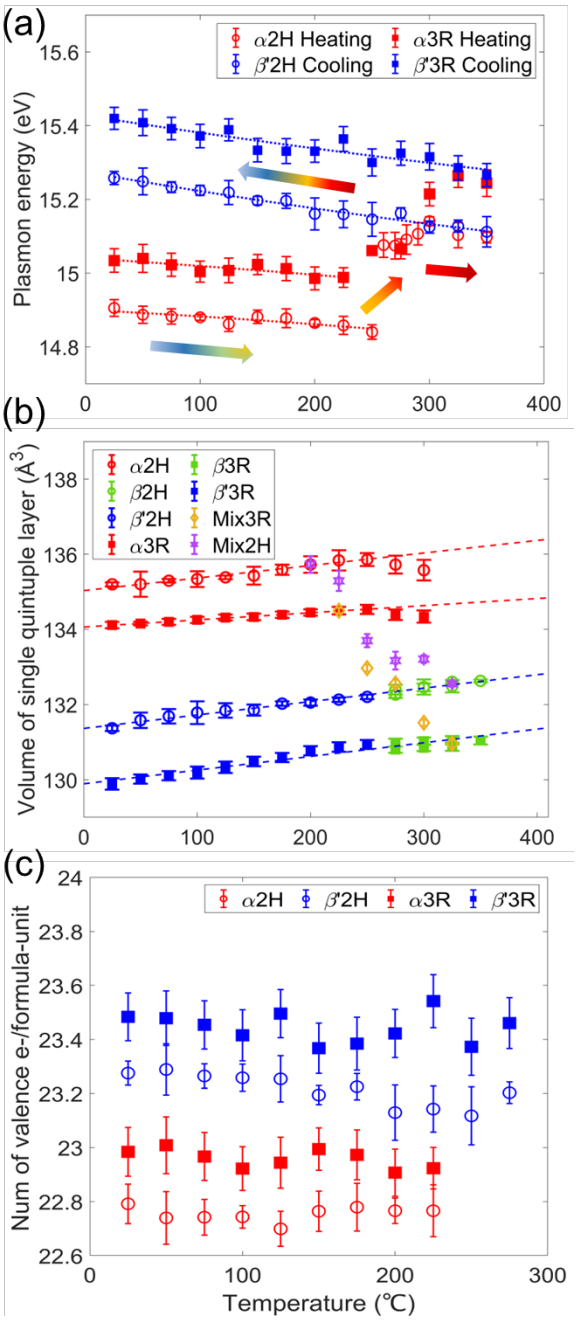

Figure 4. (a) Plasmon energies, (b) unit-cell volumes of single quintuple layers, and (c) derived numbers of valence electrons in each formula-unit volume as functions of temperature for the four In_2Se_3 phases at [0001] orientation. The arrows in (a) indicate the temperature change directions. During phase transition, the unit-cell volumes are plotted for both the individual phases (α-In_2Se_3: red, β-In_2Se_3: green) and the averaged volume from the mixture.

ASSOCIATED CONTENT

Supporting Information

The Supporting Information is available free of charge.

Experimental Methods for sample preparation, Characterization details, data analysis, and First-principles calculation, note for deriving the number of valence electrons from plasmon energies, and supplementary figures and tables.

AUTHOR INFORMATION

Corresponding Author

Ye Zhu - Department of Applied Physics, Research Institute for Smart Energy, The Hong Kong Polytechnic University, Hung Hom, Hong Kong, China; Email: yezhu@polyu.edu.hk

Xin Luo - State Key Laboratory of Optoelectronic Materials and Technologies, Guangdong Provincial Key Laboratory of Magnetoelectric Physics and Devices, Centre for Physical Mechanics and Biophysics, School of Physics, Sun Yat-sen University, Guangzhou 510275, China; Email: luox77@mail.sysu.edu.cn

Author Contributions

[+]C.C. and M.D. contributed equally to this work.

Notes

The authors declare no competing financial interest.

ACKNOWLEDGMENT

Y. Z. thanks the financial support from the Research Grants Council of Hong Kong (Project No. 15308323), the Hong Kong Polytechnic University grant (Project No. ZVRP). X.L. acknowledge the support from National Natural Science Foundation of China (Grants No. 12172386), the National Natural Science Foundation of Guangdong Province, China (Grant No. 2021B1515020021). The TEM facility is funded by the Research Grants Council of Hong Kong (Project No. C5029-18E).

REFERENCES

(1) Li, W.; Qian, X.; Li, J. Phase transitions in 2D materials. *Nat. Rev. Mater.* **2021**, *6*, 829-846.

(2) Bergeron, H.; Lebedev, D.; Hersam, M. C. Polymorphism in post-dichalcogenide two-dimensional materials. *Chem. Rev.* **2021**, *121*, 2713-2775.

(3) Peng, H.; Xie, C.; Schoen D. T.; Cui, Y. Large Anisotropy of Electrical Properties in Layer-Structured In2Se3 Nanowires. *Nano Lett.* **2008**, *8*, 1511-1516.

(4) Liu, L.; Dong, J.; Huang, J.; Nie, A.; Zhai, K.; Xiang, J.; Wang, B.; Wen, F.; Mu, C.; Zhao, Z.; Gong, Y.; Tian, Y.; Liu, Z. Atomically Resolving Polymorphs and Crystal Structures of In2Se3. *Chem. Mater.* **2019**, *31*, 10143-10149.

(5) Osamura, K.; Murakami, Y.; Tomiie, Y. Crystal Structures of α-and β-indium selenide, In2Se3. *J. Phys. Soc. Jpn.* **1966**, *12*, 1848.

(6) Popović, S.; Čelustka, B.; Bidjin, D. X‐Ray Diffraction Measurement of Lattice Parameters of In2Se3. *Phys. Status Solidi A* **1971**, *6*, 301–304.

(7) Van Landuyt, J.; Van Tendeloo, G.; Amelinckx, S. Phase transitions in In2Se3 as studied by electron microscopy and electron diffraction. *Phys. Status Solidi A* **1975**, *30*, 299–314.

(8) Popovic, S.; Tonejc, A.; Grzeta-Plenkovic, B.; Celustka, B.; Trojko, R. Revised and new crystal data for indium selenides. *J. Appl. Crystallogr.* **1979**, *12*, 416–420.

(9) Van Landuyt, J.; Van Tendeloo, G.; Amelinckx, S. New low‐temperature phase in α‐In2Se3. *Phys. Status Solidi A* **1974**, *26*, K103–K104.

(10) Ding, W.; Zhu, J.; Wang, Z.; Gao, Y.; Xiao, D.; Gu, Y.; Zhang, Z.; Zhu, W. Prediction of intrinsic two-dimensional ferroelectrics in In2Se3 and other III2-VI3 van der Waals materials. *Nat. Commun.* **2017**, *8*, 14956.

(11) Manolikas, C. New results on the phase transformations of In2Se3. *J. Solid State Chem.* **1988**, *74*, 319-328.

(12) Tao, X.; Gu, Y. Crystalline–Crystalline Phase Transformation in Two-Dimensional In2Se3 Thin Layers. *Nano Lett.* **2013**, *13*, 3501-3505.

(13) Küpers, M.; Konze, P. M.; Meledin, A.; Mayer, J.; Englert, U.; Wuttig, M.; Dronskowski, R. Controlled Crystal Growth of Indium Selenide, In2Se3, and the Crystal Structures of α-In2Se3. *Inorg. Chem.* **2018**, *57*, 11775-11781.

(14) Zhou, Y.; Wu, D.; Zhu, Y.; Cho, Y.; He, Q.; Yang, X.; Herrera, K.; Chu, Z.; Han, Y.; Downer, M. C. Out-of-Plane Piezoelectricity and Ferroelectricity in Layered α-In2Se3 Nanoflakes. *Nano Lett.* **2017,** *17*, 5508-5513.

(15) Xue, F.; Hu, W.; Lee, K. C.; Lu, L. S.; Zhang, J.; Tang, H. L.; Han, A.; Hsu, W. T.; Tu, S.; Chang, W. H.; Lien, C. H.; He, J. H.; Zhang, Z.; Li, L. J.; Zhang, X. Room-Temperature Ferroelectricity in Hexagonally Layered α-In2Se3 Nanoflakes down to the Monolayer Limit. *Adv. Funct. Mater.* **2018**, *28*, 180373.

(16) Si, M.; Saha, A. K.; Gao, S.; Qiu, G.; Qin, J.; Duan, Y.; Jian, J.; Niu, C.; Wang, H.; Wu, W.; Gupta, S. K.; Ye, P. D. A ferroelectric semiconductor field-effect transistor. *Nat. Electron.* **2019**, *2*, 580.

(17) Sun, W.; Wang, W.; Li, H.; Zhang, G.; Chen, D.; Wang, J.; Cheng, Z. Controlling bimerons as skyrmion analogues by ferroelectric polarization in 2D van der Waals multiferroic heterostructures. *Nat. Commun.* **2020**, *11*, 5930.

(18) Wang, S.; Liu, L.; Gan, L.; Chen, H.; Hou, X.; Ding, Y.; Ma, S.; Zhang, D. W.; Zhou, P. Two-dimensional ferroelectric channel transistors integrating ultra-fast memory and neural computing. *Nat. Commun.* **2021**, *12*, 53.

(19) Ding, J.; Shao, D. F.; Li, M.; Wen, L. W.; Tsymbal, E. Y. Two-dimensional antiferroelectric tunnel junction. *Phys. Rev. Lett.* **2021**, *126*, 057601.

(20) Xu, C.; Chen, Y.; Cai, X.; Meingast, A.; Guo, X.; Wang, F.; Lin, Z.; Lo, T. W.; Maunders, C.; Lazar, S.; Wang, N.; Lei, D.; Chai, Y.; Zhai, T.; Luo, X.; Zhu, Y. Two-Dimensional Antiferroelectricity in Nanostripe-Ordered In2Se3. *Phys. Rev. Lett.* **2020**, *125*, 047601.

(21) Wan, S.; Li, Y.; Li, W.; Mao, X.; Wang, C.; Chen, C.; Dong, J.; Nie, A.; Xiang, J.; Liu, Z. Nonvolatile Ferroelectric Memory Effect in Ultrathin α-In2Se3. *Adv. Funct. Mater.* **2019**, *29*, 1808606.

(22) Choi, M. S.; Cheong, B. K.; Ra, C. H.; Lee, S.; Bae, J. H.; Lee, S.; Lee, G. D.; Yang, C. W.; Hone, J.; Yoo, W. J. Electrically Driven Reversible Phase Changes in Layered In2Se3 Crystalline Film. *Adv. Mater.* **2017**, *29*, 1703568.

(23) Zheng, C.; Yu, L.; Zhu, L.; Collins, J. L.; Kim, D.; Lou, Y.; Xu, C.; Li, M.; Wei, Z.; Zhang, Y.; Edmonds, M. T.; Li, S.; Seidel, J.; Zhu, Y.; Liu, J. Z.; Tang, W.-X.; Fuhrer, M. S. Room temperature in-plane ferroelectricity in van der Waals In2Se3. *Sci. Adv.* **2018**, *4*, eaar7720.

(24) Li, W.; Sabino, F. P.; de Lima, F. C.; Wang, T.; Miwa, R. H.; Janotti, A. Large disparity between optical and fundamental band gaps in layered. *Phys. Rev. B* **2018**, *98*, 165134.

(25) Muller, D.; Silcox, J. Delocalization in inelastic scattering. *Ultramicroscopy* **1995**, *59*, 195-213.

(26) Egerton, R. F. *Electron Energy Loss Spectroscopy in the Electron Microscope*, Springer, New York, **2011**.

(27) Hu, X.; Yasaei, P.; Jokisaari, J.; Öğüt, S.; Salehi-Khojin, A.; Klie, R. F. Mapping thermal expansion coefficients in freestanding 2D materials at the nanometer scale. *Phys. Rev. Lett.* **2018**, *120*, 055902.

(28) Shen, L.; Mecklenburg, M.; Dhall, R.; Regan, B.; Cronin, S. B. Measuring nanoscale thermal gradients in suspended MoS2 with STEM-EELS. *Appl. Phys. Lett.* **2019**, *115*, 153108.

(29) Mecklenburg, M.; Hubbard, W. A.; White, E.; Dhall, R.; Cronin, S. B.; Aloni, S.; Regan, B. Nanoscale temperature mapping in operating microelectronic devices. *Science* **2015**, *347*, 629-632.

(30) Abe, H.; Terauchi, M.; Kuzuo, R.; Tanaka, M.; Temperature dependence of the volume-plasmon energy in aluminum. *J. Electron Microsc.* **1992**, *41*, 465.

(31) Meyer, G.; Über die Abhängigkeit der charakteristischen Energieverluste von Temperatur und Streuwinkel. *Z. Phys* **1957**, *148*, 61–71.

(32) Palanisamy, P.; Howe, J. M. Melting and supercooling studies in submicron Al particles using valence electron energy-loss spectroscopy in a transmission electron microscope. *J. Appl. Phys.* **2011**, *110*, 024908.

(33) Lyu, F.; Li, X.; Tian, J.; Li, Z. Liu, B.; Chen, Q. Temperature-Driven α-β Phase Transformation and Enhanced Electronic Property of 2H α-In2Se3. *ACS Appl. Mater. Interfaces* **2022**, *14*, 23637−23644.

(34) Peng, H.; Xie, C.; Schoen, D. T.; Cui, Y. Large Anisotropy of Electrical Properties in Layer-Structured In2Se3 Nanowires. *Nano Lett.* **2008**, *8*, 1511-1516.

(35) Yan, S.; Xu, C.; Zhong, C.; Chen, Y.; Che, X.; Luo, X.; Zhu, Y. Phase Instability in van der Waals In2Se3 Determined by Surface Coordination. *Angew. Chem. Int. Ed.* **2023**, *62*, e202300302.

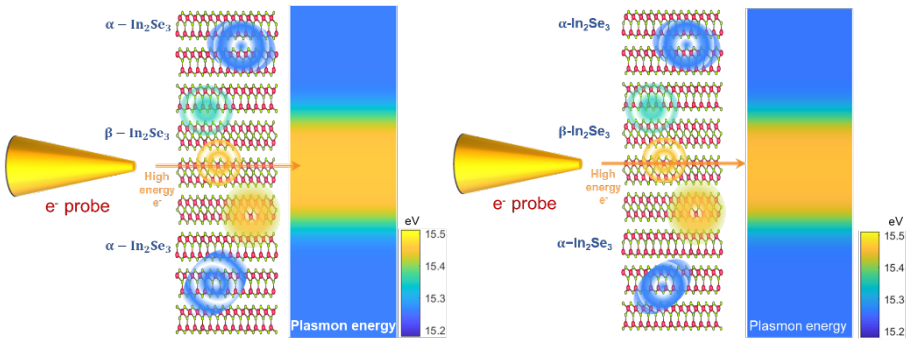

For Table of Contents Only